Translational Oncology
www.transonc.com

Volume 3 Number 6 December 2010 pp. 344–353 344

Targeted *Apc;Twist* Double-Mutant Mice: A New Model of Spontaneous Osteosarcoma That Mimics the Human Disease[1,2,3]

Natacha Entz-Werlé*,†, Philippe Choquet‡, Agnès Neuville§, Sabine Kuchler-Bopp¶, François Clauss¶, Jean-Marc Danse#, Pauline Simo-Noumbissie¶, Eric Guérin†, Marie-Pierre Gaub†, Jean-Noel Freund, Nelly Boehm††, André Constantinesco‡, Patrick Lutz*, Dominique Guenot† and Fabienne Perrin-Schmitt¶**

*Pédiatrie Onco-Hématologie, CHRU Hautepierre, Strasbourg, France; †EA 4438-UdS, « Marqueurs moléculaires de progression tumorale et de sensibilisation aux drogues anticancéreuses », Strasbourg, France; ‡Service de Biophysique et de Médecine Nucléaire, CHRU Hautepierre, Strasbourg, France; §Service de Pathologie et d'Histopathologie, Centre de Ressources Biologiques, CHRU Hautepierre, Strasbourg, France; ¶UMR977-INSERM « Biomatériaux et ingénierie tissulaire », UdS, Faculté de Médecine, Strasbourg, France; #EA3949-UdS, Faculté de Médecine, Strasbourg, France; **U682-INSERM, Strasbourg, France; ††U666-INSERM, UdS, Faculté de Médecine, Strasbourg, France

Abstract

TWIST and adenomatosis polyposis coli (*APC*) are critical signaling factors in normal bone development. In previous studies examining a homogeneously treated cohort of pediatric osteosarcoma patients, we reported the frequent and concurrent loss of both *TWIST* and *APC* genes. On these bases, we created a related animal model to further explore the oncogenic cooperation between these two genes. We performed intercrosses between *twist-null*/+ and *Apc*1638N/+ mice and studied their progeny. The *Apc*1638N/+;*twist-null*/+ mice developed bone abnormalities observed by macroscopic skeletal analyses and *in vivo* imaging. Complementary histologic, cellular, and molecular analyses were used to characterize the identified bone tumors, including cell culture and immunofluorescence of bone differentiation markers. Spontaneous localized malignant bone tumors were frequently identified in *Apc*1638N/+;*twist-null*/+ mice by *in vivo* imaging evaluation and histologic analyses. These tumors possessed several features similar to those observed in human localized osteosarcomas. In particular, the murine tumors presented with fibroblastic, chondroblastic, and osteoblastic osteosarcoma histologies, as well as mixtures of these subtypes. In addition, cellular analyses and bone differentiation markers detected by immunofluorescence on tumor sections reproduced most murine and human osteosarcoma characteristics. For example, the early bone differentiation marker Runx2, interacting physically with hypophosphorylated pRb, was undetectable in these murine osteosarcomas, whereas phosphorylated retinoblastoma was abundant in the osteoblastic and chondroblastic tumor subtypes. These characteristics, similar to those observed in human osteosarcomas, indicated that our animal model may be a powerful tool to further understand the development of localized osteosarcoma.

Translational Oncology (2010) 3, 344–353

Address all correspondence to: Pr Natacha Entz-Werlé, MD, PhD, Pédiatrie Onco-Hématologie, CHRU-Hautepierre, Avenue Molière, 67098 Strasbourg Cedex, France. E-mail: Natacha.entz-werle@chru-strasbourg.fr

[1]The authors thank the Conseil Régional d'Alsace, the Association Régionale d'Action Médicale et sociale en faveur d'Enfants atteints d'affections malignes (ARAME), the Ligue contre le Cancer and national PHRC for grants and the University of Strasbourg and the working committee on pediatric osteosarcomas in SFCE (Société Française des Cancers de l'Enfant) for support.
[2]The authors declare no conflict of interest.
[3]Following the international writing consensus, full capital letters stand for human genes, whereas lowercase letters are used for mouse genes.
Received 9 June 2010; Revised 24 August 2010; Accepted 26 August 2010

DOI 10.1593/tlo.10169

Introduction

Misexpressions of critical developmental and signaling factors seem to be decisive events in oncogenesis. In the case of osteosarcomas, our laboratory has demonstrated that several genes involved in bone development are potential oncogenes, as well as being useful prognostic markers of the clinical outcomes [1–3]. Among the genes important for bone development, we have shown that the concurrent loss of both *TWIST* and adenomatosis polyposis coli (*APC*) genes occurs in osteosarcomas of human patients with a very poor prognosis [3]. On the basis of these data, we decided to create an animal model with simultaneous loss of *Twist* and *Apc* and to demonstrate and further examine the oncogenic cooperation between these genes. We hypothesized that spontaneous osteosarcoma development would occur in the *Apc*;*twist* heterozygous progeny from an intercross between *twist-null* and *Apc* mutant mice.

Currently, the development of animal models is required to fully understand human malignant processes. To the best of our knowledge, only few murine models of osteosarcoma have been established, including genetically engineered models [4–6], irradiated mice [7], or murine and human osteosarcoma cell lines injected subcutaneously or orthotopically into nude mice [8,9]. Most of the genes implicated in these animal models play a role in the cell response to cell division signals, including transgenic mice overexpressing *cFos* [4,5] or *p53*-deficient mice [6,7,10,11]. Usually, the gene deregulations are induced artificially and/or ectopically in bones. In contrast, our target genes are generally described in differentiation pathways and are congenitally underexpressed in our model.

Twist haploinsufficiency was shown to upset bone tissue in both mice and humans [12,13] and was linked to a syndromic craniosynostosis diagnosis: the Saethre-Chotzen syndrome [14,15]. However, neither bone tumors nor malignancies have been reported in human or murine populations with the mutated *TWIST* gene. In the literature, high expression of TWIST has been described in several cancers [16–19] and has been associated with the initial phase of metastatic progression [20]. On contrast, in our homogeneous cohort of osteosarcoma patients [21], the *TWIST* gene was frequently deleted in the tumors at diagnosis, and its haploinsufficiency was significantly correlated with a poorer patient outcome and the *APC* gene loss of heterozygosity (LOH) [3].

The Apc/β-catenin/Gsk complex is the cytoplasmic transducer of the Wnt signaling pathway [22,23]. *APC* mutations lead to β-catenin accumulation and constitutive activation of Wnt-signaling targets, in the absence of Wnt inducer [24,25]. *APC* LOH is often associated with somatic mutations in the other allele, as it has been described in colon cancers [22]. However, no somatic mutations in the other *APC* allele were found in our osteosarcoma cohort, only gene deletions were observed [3].

Both *Twist* gene and Apc/β-catenin/Gsk complex positively regulate Runx2, common target of the two pathways [26,27]. Runx2 expression is reduced in cultured osteoblasts by Twist inactivation [28], whereas its repression is a consequence of the misexpression of Apc [27]. Runx2 plays a prominent role in committing mesenchymal cells toward a bone cell lineage and interacts with the hypophosphorylated form of phosphorylated retinoblastoma (pRb) to inhibit cell division [26].

In the present study, we validate our hypothesis that combined *TWIST* and *APC* gene dysfunctions cooperate in the development of osteosarcoma. For this purpose, we used *twist-null* [14] and *Apc*1638N [29] heterozygous mice as our experimental tools. The *twist-null* mouse is widely well known as a reference in the study of *Twist* gene. The *Apc* mutant mouse is known to display a relatively mild intestinal cancer phenotype and to live longer than other *Apc* mutant mice, reason why this animal strain was selected [30–32]. The *Apc*1638N/+; *twist-null*/+ mice developed spontaneously malignant bone tumors, which were characterized as osteosarcomas by *in vivo* imaging and histology. At the molecular level, we further analyze these tumors by detecting the presence of bone differentiation markers in tumor tissue sections, genotyping the tumors, performing *in vitro* and *in vivo* assays. Mechanistically, the combined *Apc*;*twist* deficit results in the decreased expression of Runx2, independently from hypophosphorylated pRb expression. With all these macroscopic and molecular characteristics, our mouse model seems to confirm the synergistic effect of *Twist* haploinsufficiency and *Wnt/β-catenin/Apc* deficiency in the malignant process of osteosarcomas.

Materials and Methods

Mouse Husbandry, Genotyping, and Skeleton Preparations

All animal experiments were performed according to French Animal Regulations. The animals were generated by crossing *twist-null* heterozygotes (on C57BL/6J and CD1 pure backgrounds for >20 generations) with *Apc*1638N heterozygotes (129Sv background). Backcrosses and intercrosses were performed to develop congenic and mixed background animals and to discriminate the phenotype because of the two studied mutant genes from the consequences of genetic modifiers, which might be present in the backgrounds. Mice were systematically genotyped by conventional polymerase chain reaction–based procedures using Eppendorf Mastercycler ep gradients (Harlow Scientific, Arlington, MA). *Twist* gene genotyping was done with primers previously described [14], whereas *Apc* genotyping was performed with primers provided by Dr R. Fodde. The *Apc* genotyping was also used to analyze tumor tissues. Same-sex littermates of the four genotypes were raised together until they were simultaneously analyzed. P0 up to 22-month-old littermate animals were collected at several generations in backcrosses. Thus, the phenotypes were studied at different levels of strain purity and background mixes (F1, F4, F8, F10, etc). To detect whether any maternal or paternal inheritance would modify the severity of the phenotype in progeny, we crossed males bearing the *Twist* mutant allele with mutant *Apc* females and reverse.

After animal sacrifice, skeletons were prepared as previously described [13].

In Vivo *Imaging Evaluation of Living Mice*

A cohort of living mice were analyzed by *in vivo* exploration. X-ray micro–computed tomography (X-ray μCT) and micro–single-photon emission computed tomography (μSPECT) were performed using a dual-modality system, the eXplore speCZT Vision 120 (GE Healthcare, London, Ontario, Canada). After anesthesia of the mice, using isoflurane in air (5% at induction then 1.5% to 2% during examination), 0.1 to 0.25 ml of Osteocis (HMDP ^{99m}Tc 74-111 MBq; CIS Bio International, Gif-sur-Yvette, France) were injected into the tail vein. A 1-hour duration was maintained between the time of injection and the μSPECT acquisitions, which were done using a cylindrical slit collimator (eight slits) or a pinhole collimator (seven pinholes). Forty-five angle positions (each lasting 20 seconds) were taken for a total acquisition time of 15 minutes. Reconstructions (energy window, 130-150 keV) were done using a three-dimensional OSEM algorithm, with reconstructed

voxels of 550 × 550 × 2460 μm^3 with the slit collimator and 330 × 330 × 330 μm^3 with the pinhole collimator. The μCT was performed using 220 projections with an angle increment of 0.877 degrees (Parker mode) and one average frame per projection (70.0 kV, 32 mA, and exposition time of 16 milliseconds). Reconstructions were done using a Feldkamp algorithm giving voxels of 100 × 100 × 100 μm^3. In case of abnormal structures, seen in the images of the first μCT acquisition, a second μCT acquisition was performed with a smaller voxel size (50 × 50 × 50 μm^3). For comparison, μCT and μSPECT images were superimposed using MicroView (GE Healthcare).

Cell Cultures

Cells from two osteosarcomas of two *Apc*1638N/+;*twist-null*/+ mice and from normal bones of *twist-null*/+, *Apc*1638N/+ and *Apc*1638N/+;*twist-null*/+ mice (2-mm^3 samples) were cultured in medium containing RPMI, Ammiomax II, 10% standard fetal calf serum, and 1% glutamine. For the agarose gel colony formation assay, two layers of 0.5% agarose (Bio-Rad, Paris, France) were used. Colony formation and expansion were enumerated after a 2-week multiplication period.

Murine Tumor Xenografting

Male athymic nude mice (6-week-old animals) were purchased from Charles River Laboratories (Chatillon-Sur-Chalaronne, France) and were maintained under pathogen-free conditions. One of the costal tumors isolated from an *Apc*1638N/+;*twist-null*/+ mouse and one cultured tumor lysate (30 × 10^6 cells) were used separately for subcutaneous injection into these immunocompromised mice. The subcutaneous tumors were measured three times a week.

Karyotyping

Standardized mouse karyotyping was performed, and computer-assisted karyotyping was used to compare bone tumor and control mouse cells.

Histology

Soft tissue and bone tumors isolated after *in vivo* imaging were fixed in 4% formaldehyde. The bone specimens were decalcified and paraffin-embedded for histologic analyses. All tumors were stained with hematoxylin and eosin (Sigma, St. Quentin, France). Serial sections (5 μm) were obtained from eight murine osteosarcomas, which were chosen because of their large size, allowing to perform all protein analyses. These eight bone tumors were isolated from eight different *Apc*1638N/+;*twist-null*/+ mice.

Analyses of Protein Expression by Immunofluorescence

Standard protocols were used to deparaffinize the mouse tumor serial sections. Slides were saturated with 1% bovine serum albumin in 1× phosphate-buffered saline (PBS) and incubated with antibody for 2 hours at room temperature. Rabbit anti–β-catenin (SC199), anti-RankL (SC9073) and anti-Runx2 (SC10758), goat anti-osteonectin (SC13326), anti-*Col1A1* (SC25974), anti-osteocalcin (SC18322), and anti-pRb (SC16671) (Santa Cruz Biotechnology, Heidelberg, Germany) were incubated on tissue sections at dilutions ranging from 1:100 to 1:800. After washing with PBS to remove background, 1:100 or 1:200 dilutions of Alexa 488– and/or Alexa 594–coupled antirabbit or antigoat secondary antibodies (Invitrogen, Cergy Pontoise, France) were used for immunodetection. Incubations with 4′,6′-diamidino-2-phenylindole (Sigma) were used to detect the nuclei. Detections of pRb and Runx2 were done after antigen retrieval and 2.5% Triton permeabilization of the tissue sections. Control slides were obtained by replacing the primary antibodies with PBS.

Results

Generation of Apc1638N/+;twist-null/+ Mice

Mice combining haploinsufficiency of *Twist* and heterozygous for the *Apc*1638N allele, referred hereafter as the *Apc*1638N/+;*twist-null*/+ mice, are the progeny of an intercross between *twist-null* and *Apc*1638N heterozygotes. Littermates from more than 90 crosses were genotyped, and no developmental lethality was observed as almost equivalent numbers of living pups for each of the four genotypes. From a total number of 530 animals, 29% (154/530) were wild-type (WT), 25% (133/530) were *twist-null*/+, 26% (137/530) were *Apc*1638N/+, and 20% (106/530) were *Apc*1638N/+;*twist-null*/+. Among them, 253 females and 277 males were numbered. The intercrosses were initially produced using pure CD1 and C57BL/6J backgrounds for *twist-null*/+ animals and a 129Sv background for *Apc*1638N/+. Backcrosses and intercrosses were regularly performed in subsequent generations. Of the first 530 animals, we observed 182 animals with CD1 background, 175 mice presenting C57BL/6J background, and 173 mice with 129Sv background.

Apc1638N/+;twist-null/+ Mice Have Soft Tissue and Bone Abnormalities Similar to Those of the Apc1638N/+ and Twist-null/+ Heterozygotes

*Apc*1638N/+ mice have been reported to develop intestinal cancers and extraintestinal manifestations [29,30,32]. Macroscopically, soft tissue tumors were approximately two times as frequent in *Apc*1638N/+;*twist-null*/+ mice than in *Apc*1638N/+ mice. No soft tissue tumors were observed in any of the *twist-null*/+ animals. Histology classified these soft tissue tumors as desmoid and keratinoid tumors. No malignant tumors were observed in the intestines in any of the mice from all four genotypes. Of all animals, 13 spontaneous adenomas were found in 73 examined *Apc*1638N/+;*twist-null*/+ animals and 21 were found in 112 examined *Apc*1638N/+ mice.

In terms of the bones, we analyzed the complete skeletons of the 73 of 106 *Apc*1638N/+;*twist-null*/+ mice that were, first, generated. In full agreement with our previous unpublished studies of the *twist* haploinsufficient phenotype and, beside secondary bone anomalies reported in previous publications [13,15], the major specific bone features were a complete bilateral or unilateral coronal suture fusion and bilateral or unilateral posterior hallux duplications, occurring as a fully penetrant phenotype in C57BL/6J background. These observations were present in the *Apc*1638N/+;*twist-null*/+ animals, as well as for the *twist-null*/+ mice with this background, whereas on animals with a CD1 background, no duplication of the halluces was observed, and coronal sutures were only partially fused.

Bone Tumors Are Limited to the Apc1638N/+;twist-null/+ Mice

In addition to the bone phenotype specific of the *twist-null*/+ heterozygotes, 14 (19.2%) of the 73 analyzed *Apc*1638N/+;*twist-null*/+ skeletons presented bone tumors, which were mostly found in the cephalic region (Figure 1). The earliest tumors were seen in the 5-month-old *Apc*1638N/+;*twist-null*/+ mice (Table 1). They were frequently associated with one or two other bone tumors at other bone locations: in more than 70% (10 mice), an average of two concomitant tumors was observed. On the basis of these initial results, we limited

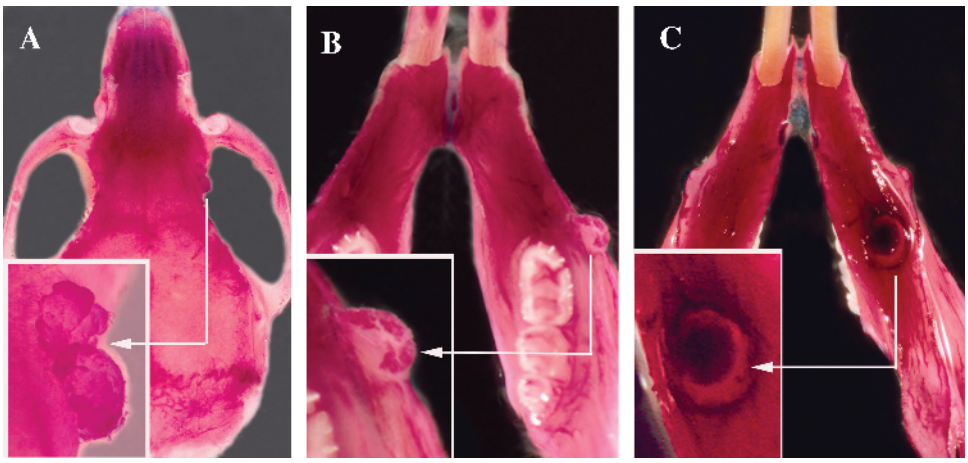

Figure 1. Malignant abnormalities observed in skeletal preparations from *Apc*1638N/+;*twist-null*/+ mice. (A) Upper side view of the skull (0.6×) from a 9-month-old female and focus on a tumor located at the junction of the external and orbital surface of the right frontal bone (insert at 1.2×). (B) Upper side view of the mandible from a 5-month-old mouse (0.75×) and focus on the extraosseous extension on the lateral side of the right mandible (insert at 1.5×). (C) Lower side view of the mandible from a 5-month-old mouse (0.75×) and focus on the osteolytic tumor located on the lower side of the left mandible (insert at 1.5×).

our analyses to the cephalic region, where the tumors were predominantly seen. We generated 92 new *Apc*1638N/+;*twist-null*/+ animals, aged between 5 and 22 months, when they were killed. In this population, tumor development occurred in 30 (32.6%) of 92 cephalic structures. The size of the tumors did not correlate with the age of the animal at the time of examination. In addition, there were no differences in the penetrance of the bone tumors between sexes and backgrounds. No bone tumors were seen in the WT or the *twist-null*/+ mice. Of the 112 initial *Apc*1638N/+ animals, 3 presented a bone outgrowth, histologically similar to osteomas.

The skeleton analyses allowed us to estimate the penetrance of bone tumors on a large population. To go further, an *in vivo* imaging evaluation was performed in a smaller cohort of living animals because of its complexity.

In Vivo *Imaging and Histologic Analyses Confirm the Murine Bone Tumors as Osteosarcomas*

To localize precisely the tumors and to obtain subsequently tumor tissues, a small cohort of mice were newly generated. Among them, 22 *Apc*1638N/+;*twist-null*/+ mice and 22 control animals, pooling *Apc*1638N, *twist-null*, and WT mice, were selected based on age (between 10 and 18 months). In the *Apc*1638N/+ murine population, the selection was also based on the presence of multiple soft tissue tumors. All animals were analyzed by X-ray μCT and μSPECT. After animal sacrifice, each tumor, which was diagnosed by *in vivo* imaging, was dissected and fixed for histologic analyses. Bone tumors were detected by X-ray μCT in 15 (68.2%) of the 22 *Apc*1638N/+;*twist-null*/+ mice (Table 1). Among the 15 mice with bone tumors, 6 were injected with an osteocis tracer, whose strong uptake revealed an increased osteoblastic activity, witness of the malignant component. Lesions were present at all bone sites, including head, trunk, and appendages (Figure 2, *A*, *C*, *D*, *E*, and *F*).

In the cephalic region, tumors had an osteolytic aspect (Figure 2, *A-1*, *A-3*, and *B-1*), which was linked to a highly active tracer fixation (Figure 2, *A-2* and *B-2*), or a dense component (Figure 2, *C-1–3*). Histologically, the osteolytic lesions were characterized as fibroblastic osteosarcomas (Figure 2, *A-4* and *B-4*). In Figure 2*B-1*, the osteolytic bone tumor was presenting calcifications in the soft tissue extension, witness of an osteoblastic subtype at histologic diagnosis (Figure 2*B-3*). In Figure 2*C-4*, the dense tumor presented no tracer fixation and revealed a chondroblastic osteosarcoma. Two animals were followed by μCT at an interval of 3 months, and the volume of the tumors was measured by segmentation. In one animal, the two tumors increased by 88% and 93%, respectively (Figure 2, *C-1* and *C-2*). In the second mouse, the tumor grew by 66%. On the trunk, tumors were dense and located on costal segments (Figure 2*D*), where the histologies confirmed chondroblastic osteosarcomas. In 2 of 15 tumor-positive mice, the bone lesions were located in the forearm. One was having an osteolytic aspect and was histologically characterized as an osteoblastic osteosarcoma (Figure 2*E*). The second one was characterized by a dense aspect with a high radioactive uptake and was defined as a chondroblastic subtype (Figure 2*F*).

Of the 15 animals that presented with a positive μCT, 7 had two concomitant bone tumors and 3 had three concomitant osteosarcomas. The bone tumors were predominantly dense lesions when localized to flat bones, one third had an osteolytic μCT aspect, and occasionally, both

Table 1. Numerical Characteristics of Animals Presenting Bone Tumors (Age and Background in Each Studied Group).

*Apc*1638N/+;*twist-null*/+ Mice	Animal Number Presenting Bone Tumors	Animal Number Presenting Bone Tumors by Age			Animal Number Presenting Bone Tumors by Background		
		5-9 mo	10-15 mo	16-22 mo	CD1	C57BL/6J	129Sv
73 skeletons	14	6	3	6	6	4	4
92 cephalic regions	30	6	12	12	9	13	8
22 living animal (*in vivo* imaging)	15	0	7	8	5	4	6

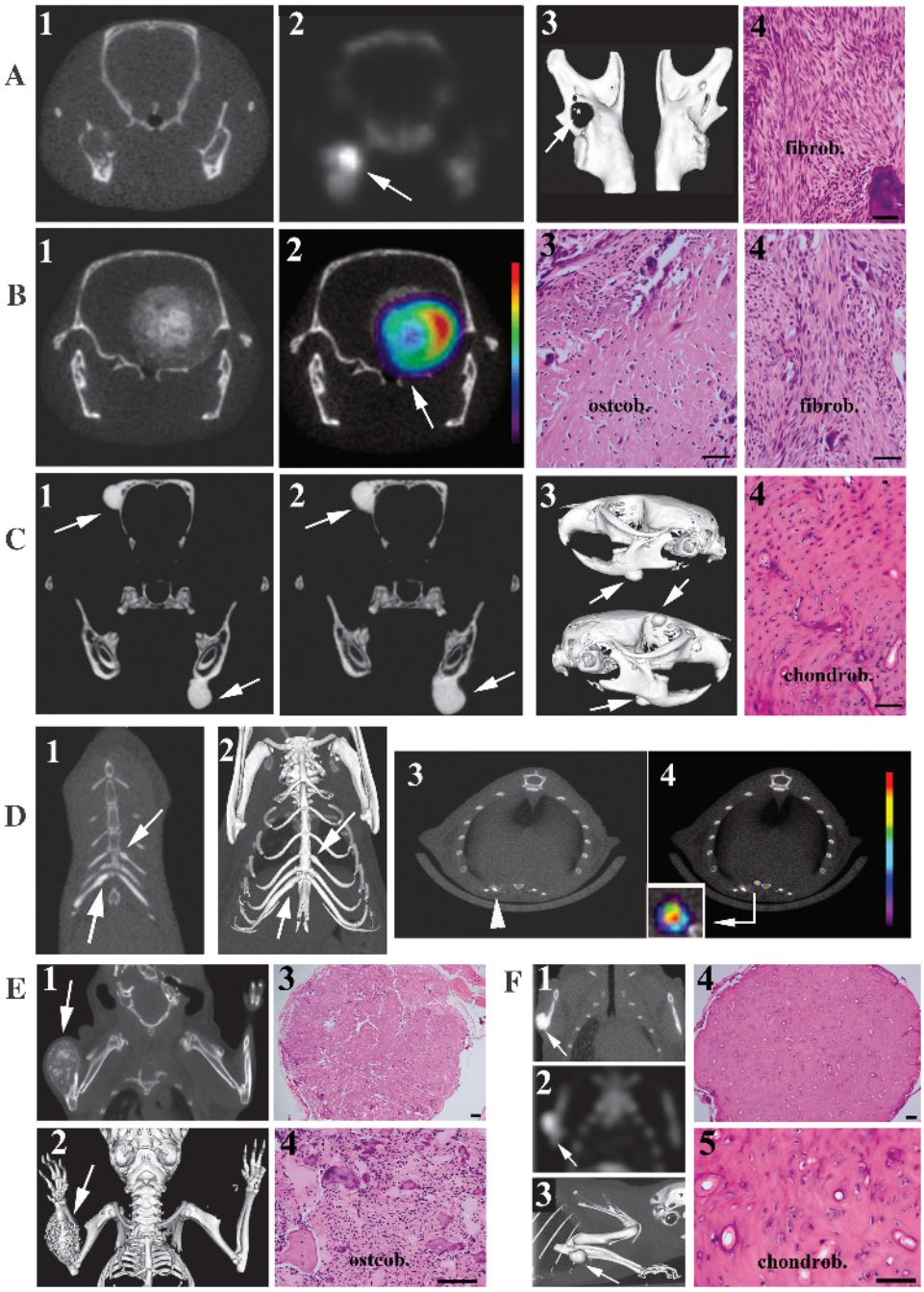

Figure 2. *In vivo* imaging evaluation and histologic analyses of osteosarcomas in *Apc*1638N/+;*twist-null*/+ mice. (A) Frontal μCT (A1), μSPECT (A2), and three-dimensional (3D) reconstruction (A3) images of the mandibles from a 14-month-old mouse reveal an osteolytic tumor on the right mandible (arrow on A3) with an active radioactivity uptake (arrow on A2). The histologic analysis (A4) shows a fibroblastic osteosarcoma (fibrob). (B) Frontal μCT (B1) and μSPECT (B2) analyses reveal an invasive tumor on the occipital bone (arrow on B2). Within this bulky tumor, the most active region is the peripheral area in red. The histology emphasizes the mixed nature of the tumor with both osteoblastic (B3, osteob) and fibroblastic (B4, fibrob) subtypes. (C) Frontal μCT (C1) and three-dimensional reconstruction (C3) analyses of two bone tumors on the left mandible and on the right parietal bone (arrows on C1, C2 and C3). The analysis of the tumors taken 3 months later shows an increase in the volume of the tumors (C2). Histology (C4) illustrates that this tumor is a chondroblastic osteosarcoma (chondrob). (D) The μCT analysis (D1) and three-dimensional reconstruction (D2) from an *Apc*1638N/+;*twist-null*/+ mouse reveal dense tumors on the fifth left and seventh right ribs (arrows). μCT (D3) and μSPECT (D4) images from another *Apc*1638N/+;*twist-null*/+ mouse reveal a lesion at the sternocostal junction on the sixth left rib (arrow on D3) with a high osteoblastic activity in the soft tissue extension on the dorsal region of this lesion (D4 and focus insert on D4). (E) μCT image of a bulky osteolytic tumor on the right forearm (E1) and three-dimensional reconstruction (E2) allow an estimate of its soft tissue extension. The histologic analysis (E3, $\times$10; E4, $\times$40) shows an osteoblastic osteosarcoma (osteob). (F) The μCT and the μSPECT analyses of another Apc1638N/+;*twist-null*/+ mouse show a dense bone tumor on the right ulna (F1) with a high radioactive uptake (F2) and its three-dimensional reconstruction (F3). Histologic analyses reveal that this lesion is a chondroblastic osteosarcoma (chondrob) (F4, $\times$10; F5, $\times$40). The bars on histologic slides represent 40 μm.

imaging presentations were present. The bone tracer uptake was present in the dense and in the osteolytic processes (Figure 2*A-2*, *B-2*, and *D-4*). Two tumors had soft tissue extensions (Figure 2, *B-2* and *D-4*). Histologically, all bone tumors were typically characterized by the presence of chondroblastic, fibroblastic, and/or osteoblastic cells and an osteoid component. The lungs were completely normal as determined by our μCT resolution. No tumors were observed in the 22 control mice, which were evaluated in parallel.

Complementary In Vivo *and* In Vitro *Experiments Assess the Malignant Features of These Murine Osteosarcomas*

Cells from two different bulky tumors were cultured because of availability of material. Although these tumor cells grew slowly, they had immortalized cell properties, as they continued to grow and divide indefinitely *in vitro*. In contrast, cells from the normal bone of the same mouse and from control mice (WT, *Apc*1638N/+, and *twist-null*/+) did not grow. The osteosarcoma cells of both tumors possessed elongated stellate cytoplasmic processes (Figure 3*A*) until they reached confluence, as previously described in human osteosarcoma cell lines [33]. A standard soft-agar colony formation assay also confirmed the malignant properties of these tumor cells, as well as the tumor xenografts. In fact, tumors at the sites of tumor cell injection grew during a period of 3 months, and histology showed similar features to those described for the murine primary osteosarcomas. Because human osteosarcomas have a highly rearranged karyotype, we also karyotyped the cultured murine tumor cells. However, the karyotype of these murine tumor cells appeared normal (Figure 3*B*). In parallel, *Apc* allele genotyping on the genomic DNA isolated from normal bones and eight murine bone tumors was performed. It revealed that the tumor cells had lost the wild-type *Apc* allele in two murine osteosarcomas (T1 and T2 in Figure 3*C*).

Concomitant Decreased Expression of Twist and Deregulation of Apc/β-Catenin Seem to Alter pRb/Runx2 Cooperation

Next, we wanted to understand the mechanism underlying the dysfunction of our two target genes, *Twist* and *Apc*. To detect the presence of discriminating markers, we performed immunofluorescence on serial sections from eight paraffin-embedded osteosarcomas prepared from eight *Apc*1638N/+;*twist-null*/+ mice. We analyzed the Wnt signaling pathway, in which Apc and β-catenin are involved, bone cell lineage differentiation markers (collagen 1, osteonectin, osteocalcin, and Runx2), and pRb, interacting with Runx2.

The data obtained from tumor T38 (a chondroblastic osteosarcoma) and from tumor T45 (a fibroblastic osteosarcoma) are shown in Figure 4, *A* and *B*, respectively. Phase-contrast images at the extreme left illustrate the morphologic differences between the healthy bone and the T38 chondroblastic osteosarcoma and show the aspect of T45 fibroblastic tumor. β-Catenin staining was nuclear in seven murine osteosarcomas (as in the T38; Figure 4*A*), whereas it was located in the nucleocytoplasmic area of the tumor cells from T45 (Figure 4*B*). Other bone differentiation markers were analyzed, including collagen1 (a marker of poorly differentiated osteoblasts), osteonectin (an early-stage osteoprogenitor marker), and osteocalcin (a marker of mature osteoblasts). In the T38 osteosarcoma cells, collagen1 and osteonectin were mostly nuclear, whereas osteocalcin staining was detected in the healthy bone and at the border between malignant osteoblasts and the malignant osteoid matrix (Figure 4*A*). Immunofluorescence analyses of the T45

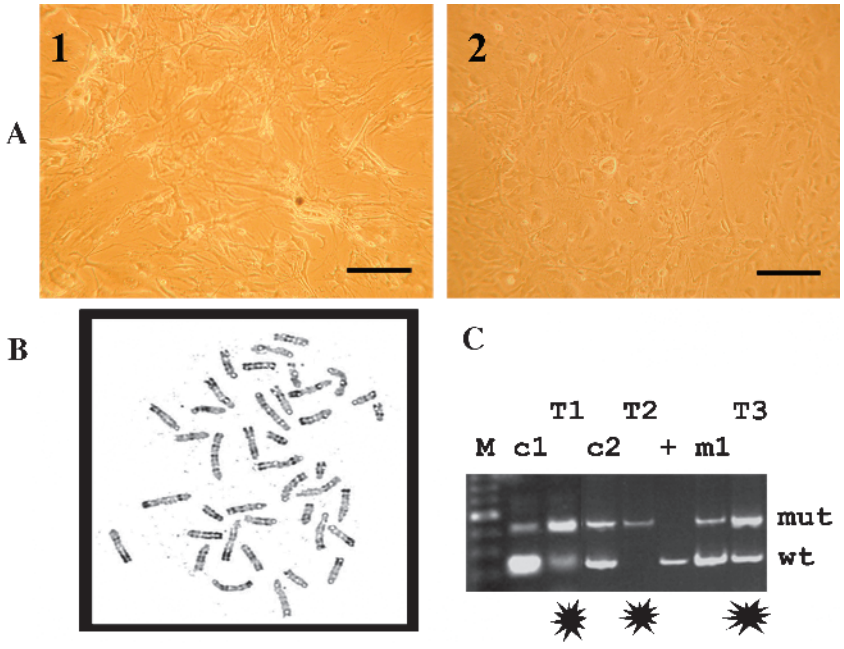

Figure 3. Cell culture, karyotype, and LOH analyses of the murine osteosarcomas. (A) Cultured cells from two different murine osteosarcomas (A1 and A2) presented elongated stellate cytoplasmic processes. (B) A normal tumor karyotype is observed in the murine osteosarcoma of an *Apc*1638N/+;*twist-null*/+ mouse. (C) *Apc* genotyping shows reversed balance of mutant and wild-type bands in the controls (c1 and c2) and the tumor (T1, T2, and T3) specimens. In T1 and T2, the mutant *Apc* allele is predominant and revealed an *Apc* loss of heterozygosity in these tumor cells of *Apc*1638N/+;*twist-null*/+ mice. The c1 and c2 specimens are normal bone DNA from the same mice. The + sample is a *Apc*1638N/+ bone tissue DNA, whereas m1 DNA was extracted from a *Apc*1638N/+;*twist-null*/+ mouse without any osteosarcoma development. M represents the size markers used for the electrophoresis.

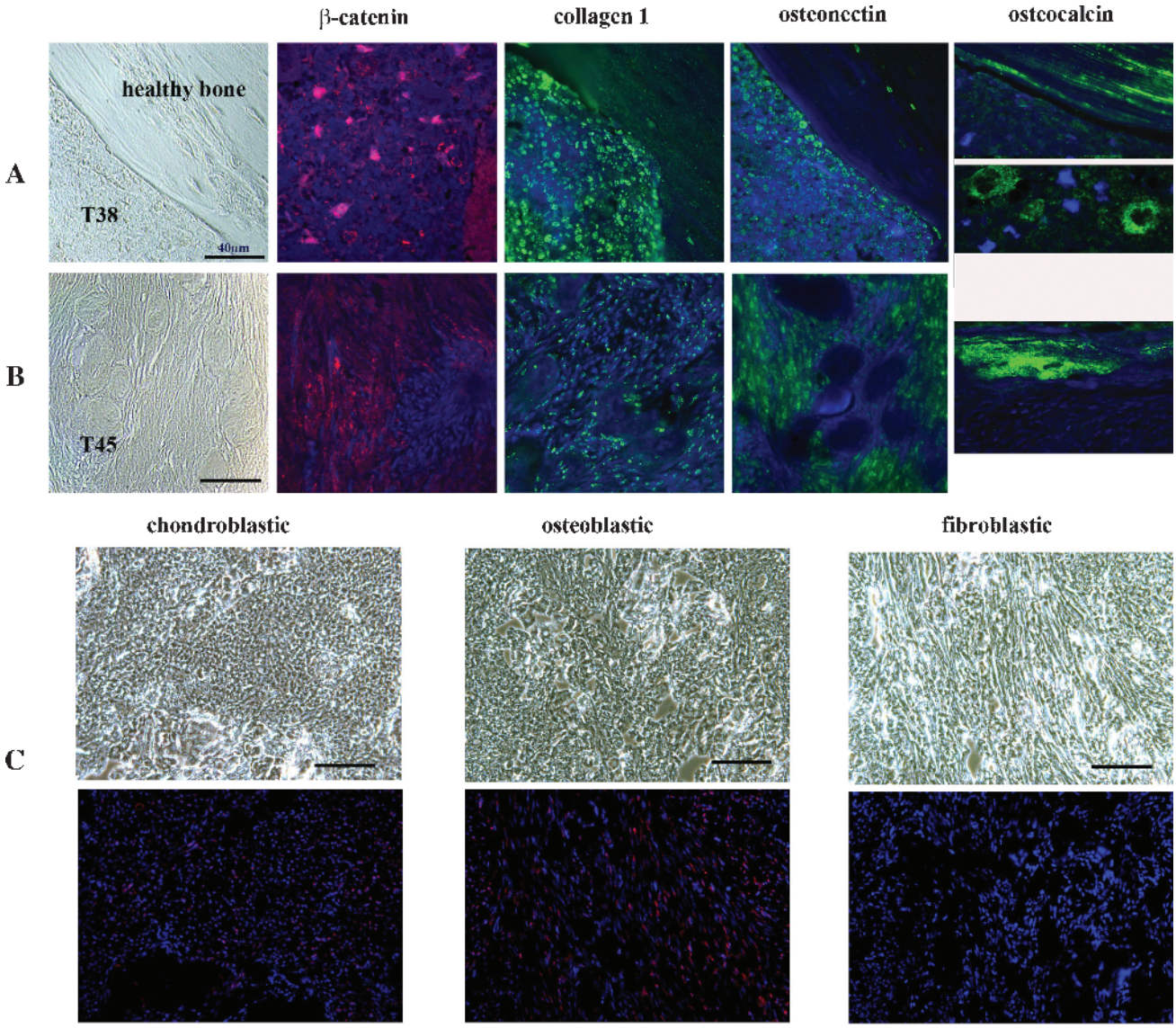

Figure 4. Molecular signature of murine osteosarcomas combining *Apc* and *twist* haploinsufficiencies. (A) On the upper row, phase-contrast imaging (at the extreme left) and immunofluorescence staining of markers were performed on sections from a dense chrondroblastic osteosarcoma in the mouse named 38 (T38). Immunofluorescent detection of β-catenin is indicated by the red signaling located mainly within the T38 nuclei. Beside this figure, the collagen1 staining, which is labeled in green, is observed in the nuclei of tumor cells but also as parallel sheets in the healthy bone. Osteonectin, labeled in green on the fourth figure of the row A, is localized within the nuclei of T38 cells, whereas osteocalcin (at the extreme right of row A) is strongly green-labeled in the healthy part of the section (figure at the top and at the extreme right of row A) and at the border between malignant osteoblasts and the malignant osteoid matrix of T38 tumor (figure below and at the extreme right of row A). (B) On the second row, an osteolytic tumor (T45, a fibroblastic osteosarcoma from mouse named 45) is shown. As in row A, the phase-contrast image of row B is at the extreme left, followed by the immunofluorescence staining. The detection of β-catenin, labeled in red, is mainly located in the nuclei and the cytoplasms of T45 cells (second image of row B), whereas collagen1 staining in green is only observed in the nuclei of tumor cells (third image of row B). The fourth image represents the osteonectin green immunofluorescence, localized in the nucleocytoplasm compartment of T45 cells, whereas osteocalcin, labeled also in green, is undetectable in T45 tumor cells. An osteocalcin staining is present in the healthy bone section of T45 section. For panels A and B, DAPI, which labels the DNA, is indicated by the blue signal and is superimposed on the green or the red signals. (C) The detection of pRb, labeled usually in red, was performed in a chondroblastic (at the extreme left), in an osteoblastic (in the middle) and in a fibroblastic (at the extreme right) murine osteosarcoma. Phase-contrast images of the tumors are shown on the top of row C. DAPI, which stains the DNA, is indicated by the blue signal and is superimposed on the red pRb signal. In the chondroblastic osteosarcoma subtype, only a weak, diffuse nuclear signal of phosphorylated pRb is detected, whereas in the osteoblastic osteosarcoma, an accumulation of phosphorylated pRb is present in both nuclear and cytoplasmic compartments. No expression of pRb is observed in the fibroblastic subtype. The bars represent 40 μm on the different figures.

fibroblastic tumor revealed sparse collagen1 staining in the nuclei, osteonectin staining in both nuclear and cytoplasmic compartments, and no detection of osteocalcin, which was only observed in the healthy bone (Figure 4*B*, *right side*).

We also investigated the presence of Runx2, which is a common target of activated β-catenin and Twist. Our attempts to detect Runx2 were negative in seven of eight tumors (data not shown). In only one tumor, comprising a mix of osteoblastic and fibroblastic osteosarcoma

cells, a weak Runx2 staining in the tumor nuclei was observed. Runx2 is known also to physically interact with the hypophosphorylated form of pRb [26,34], which has been implicated in osteoblast differentiation in human and murine osteosarcomas [1,6,7]. In Figure 4*C*, the phase-contrast images show the three different histologic subtypes of osteosarcomas on the upper row and the corresponding red signal of phosphorylated pRb superimposed on 4′,6′-diamidino-2-phenylindole staining on the lower row. In the murine chondroblastic osteosarcoma, only a weak, diffuse nuclear signal of phosphorylated pRb (Figure 4*C*, *left*) was detected, whereas in the osteoblastic form, an accumulation of phosphorylated pRb was observed in both nuclear and cytoplasmic compartments (Figure 4*C*, *middle*). In the fibroblastic osteosarcoma, no detectable phosphorylated pRb was showed (Figure 4*C*, *right*).

Discussion

Here we report a mouse model, which develops spontaneously osteosarcomas without necessity of any inducing treatment. In fact, our model develops osteosarcomas as a consequence of simultaneous and congenitally haplodeficiencies of the signaling factors *Twist* and *Apc*.

The Apc1638N/+;twist-null/+ Mice Recapitulate Features of Each Parent and Also Develop Spontaneous Osteosarcomas

*Apc*1638N/+;*twist-null*/+ mice developed the same nonmalignant soft tissue tumors than *Apc*1638N/+ mice [29–31], as well as bone dysmorphic features specific of the *twist-null*/+ mutant [13–15].

In addition, osteosarcomas were particularly observed in the rostral region, and they are probably reminiscent of the predominant cephalic dysmorphologies previously described in *twist-null*/+ mice [13,14,35] and of the previously published murine osteosarcoma models [4–7]. Tumor penetrance in *Apc*1638N/+;*twist-null*/+ mice (19.2%-32.6% as determined by skeleton observations and 68.2% by *in vivo* imaging) is significantly higher than those described for spontaneous malignant bone tumors in various other inbred and hybrid mice (range from 0.3% to 7%) [36,37]. The frequency of osteosarcoma development in the *Apc*1638N/+;*twist-null*/+ mice points toward a synergy between the combined functional deficits of *Twist* and *Apc*. Statistical differences in tumor frequency between the skeletal observations and *in vivo* imaging evaluation may be linked to the selection of the animals: the mice, imaged *in vivo*, were an older group of mice, and they also presented with more soft tissue tumors. The concurrent haploinsufficiencies at *Twist* and *Apc* seem to be genetic conditions, which favor the apparition of osteosarcomas at a relatively high frequency, but they seem not to be sufficient conditions, as every *Apc*1638N/+;*twist-null*/+ mice do not develop osteosarcomas.

At the time of examination, no lung metastases were detected, although human osteosarcomas are reported to be frequently a metastatic disease [38]. However, the μCT resolution used in the present study is not able to detect microscopic lung metastases. In addition to species-specific differences between humans and mice, one hypothesis is that abnormalities at *Twist* plus *Apc* would represent the initial genetic conditions that might favor the initiation of osteosarcoma but is not sufficient to allow progression toward a metastatic lung disease.

Molecular Alterations of Our Murine Tumors Resemble to Those of Human Osteosarcomas

The data on protein expression and cell culture characteristics are typical of those described in human osteosarcoma cell lines [8]: all chondroid and immature osteoblast markers (collagen1, osteocalcin, and osteonectin) are present in the chondroblastic subtype and are modulated differently in the fibroblastic subtype. These data are supported by the fact that fibroblastic osteosarcoma cells would present fewer late osteoblastic differentiation markers, as in the human disease [39–41]. Furthermore, β-catenin localization resembles to what has been described in human colon cancer [42], when *Apc* is deleted, and confirms the constant role of the Apc/β-catenin pathway in our model.

In addition, the absence of Runx2 detection in our murine tumors was consistent with the nuclear location of β-catenin and the decrease in Twist expression [26,34,43]. This Runx2 down-regulation was similar to the published results in human localized osteosarcomas, where they confirmed that normal Runx2 function is incompatible with the osteoblast malignant transformation [34]. Furthermore, a correlation between high *Runx2* re-expression and the metastatic disease might explain the absence of metastatic disease in our model [44]. In normal osteoblasts, Runx2 physically interacts with the hypophosphorylated form of pRb [34]. In our murine osteosarcomas, phosphorylated pRb expression was present in the chondroblastic and osteoblastic subtypes, explaining their high mitotic activity. In contrast, no phosphorylated pRb was detected in murine fibroblastic osteosarcoma. *RB* inconstant role was also demonstrated in our cohort of patients with osteosarcoma, concomitantly lacking *APC* and *TWIST* genes [1]. In the *Apc*1638N/+;*twist-null*/+ mice, osteosarcoma development might be linked to the concomitant and predominant roles of *Apc* and *Twist* deregulation on Runx2 expression, without an absolute requirement of phosphorylated pRb.

Could the Apc1638N/+;twist-null/+ Mouse Be a Good Osteosarcoma Mouse Model to Study the Human Localized Disease?

Most of the bone tumors observed in our mouse model clearly reproduced the imaging characteristics of human osteosarcomas. However, a large number of predominantly dense images could be seen in our murine osteosarcomas, as it is frequently the case in craniofacial human osteosarcomas [41,45]. This location is not common in humans, but it has been observed in other mouse models, where osteosarcomas are mostly localized to the skull. Additional human osteosarcoma features, shown in our model, include the appearance of the three typical histologic subtypes (osteoblastic, fibroblastic, and chondroblastic), as well as a mix of the three subtypes. The observed histologic subtypes are linked to the tumor locations, as in the human disease [45–47]. So, the bone tumors in our *Apc*1638N/+;*twist-null*/+ mice, which are primarily located in the head and the jaw, are predominantly diagnosed as chondroblastic osteosarcomas. Furthermore, *in vivo* imaging evaluation was also partially correlated, as in human osteosarcomas, to these histologic differences. In fact, chondroblastic tumors mostly presented a dense radiologic aspect (examples in Figure 2, *C* and *F*), whereas the osteolytic aspect was mostly linked to the osteoblastic and/or fibroblastic histologic components (examples in Figure 2, *B* and *E*).

At the molecular level, the observed *Apc* LOH in the murine tumors underlined the presence of probable discrete genomic malignant molecular features acquired in these cells and was concordant with the *APC* LOH observed in the human osteosarcomas [3]. As a normal karyotype is observed, the detected *Apc* LOH suggests that only small alterations might be sufficient for osteosarcoma formation in our model but not for its progression as a lung metastatic disease. It is then possible that major chromosomal rearrangements and lung metastases will only appear at a later step of tumor progression as a consequence of the dysfunction of an additional gene.

In conclusion, our mouse model seems to confirm the combined role of *Twist* and *Apc* genes in the development of murine malignant osteoblasts and will provide new opportunities to understand further human osteosarcomas.

Acknowledgments

The authors thank the contribution of J.N. Freund (Inserm-U381, Strasbourg) who shared the *Apc*1638N/+ mice provided by R. Fodde and S. Robine (Inserm-UMR144, Paris) and Dr F. René (Inserm-U692) for the anti-pRb antibodies. The authors also thank A. Dierich (IGBMC, Strasbourg) and E. Flori (Cytogenetics, Strasbourg) for their help in karyotyping. The authors appreciate the technical assistance of C. Lasthaus, M. Jaillet, and A. Chassepot. The authors also thank Diana Stempak, research associate, working at the University of Toronto, for her help in the manuscript writing. The authors also had the help of two reviewers of the American Journal Expert Web service.

References

[1] Entz-Werlé N, Schneider A, Kalifa C, Voegeli AC, Tabone MD, Marec-Berard P, Marcellin L, Pacquement H, Terrier P, Boutard P, et al. (2003). Genetic alterations in primary osteosarcoma from 54 children and adolescents by targeted allelotyping. *Br J Cancer* **88**, 1925–1931.

[2] Entz-Werlé N, Stoetzel C, Berard-Marec P, Kalifa C, Brugiere L, Pacquement H, Schmitt C, Tabone MD, Gentet JC, Quillet R, et al. (2005). Frequent genomic abnormalities at TWIST in human pediatric osteosarcomas. *Int J Cancer* **117**, 349–355.

[3] Entz-Werlé N, Lavaux T, Metzger N, Stoetzel C, Lasthaus C, Marec P, Kalifa C, Brugieres L, Pacquement H, Schmitt C, et al. (2007). Involvement of MET/TWIST/APC combination or the potential role of ossification factors in pediatric high-grade osteosarcoma oncogenesis. *Neoplasia* **9**, 678–688.

[4] Wang ZQ, Liang J, Schellander K, Wagner EF, and Grigoriadis AE (1995). C-*fos*–induced osteosarcoma formation in transgenic mice: cooperativity with c-*jun* and the role of endogenous c-*fos*. *Cancer Res* **55**, 6244–6251.

[5] Sunters A, McCluskey J, and Grigoriadis AE (1998). Control of cell cycle gene expression in bone development and during c-Fos–induced osteosarcoma formation. *Dev Genet* **22**, 386–397.

[6] Walkley CR, Qudsi R, Sankaran VG, Perry JA, Gostissa M, Roth SI, Rodda SJ, Snay E, Dunning P, Fahey FH, et al. (2008). Conditional mouse osteosarcoma, dependant on p53 loss potentiated by loss of Rb, mimics the human disease. *Genes Dev* **22**, 1662–1676.

[7] Berman SD, Calo E, Landman AS, Danielian PS, Miller ES, West JC, Fonhoue BD, Caron A, Bronson R, Bouxsein ML, et al. (2008). Metastatic osteosarcoma induced by inactivation of Rb and p53 in the osteoblast lineage. *Proc Natl Acad Sci USA* **105**, 11851–11856.

[8] Ek ET, Dass CR, and Choong PF (2006). Commonly used mouse models of osteosarcoma. *Crit Rev Oncol Hematol* **60**, 1–8.

[9] Dass CR, Ek ET, and Choong PF (2007). Human xenograft osteosarcoma models with spontaneous metastasis in mice: clinical relevance and applicability for drug testing. *J Cancer Res Clin Oncol* **133**, 193–198.

[10] Olive KP, Tuveson DA, Ruhe ZC, Yin B, Willis NA, Bronson RT, Crowley D, and Jacks T (2004). Mutant p53 gain of function in two mouse models of Li-Fraumeni syndrome. *Cell* **119**, 847–860.

[11] McAllister KA, Houle CD, Malphurs J, Ward T, Collins NK, Gersch W, Wharey L, Seely JC, Betz L, Bennett LM, et al. (2006). Spontaneous and irradiation-induced tumour susceptibility in BRCA2 germline mutant mice and cooperative effects with a p53 germline mutation. *Toxicol Pathol* **34**, 187–198.

[12] Stoetzel C, Weber B, Bourgeois P, Bolcato-Bellemin AL, and Perrin-Schmitt F (1995). Dorso-ventral and rostro-caudal sequential expression of M-twist in the postimplantation murine embryo. *Mech Dev* **51**, 251–263.

[13] El Ghouzzi V, Le Merrer M, Perrin-Schmitt F, Lajeunie E, Benit P, Renier D, Bourgeois P, Bolcato-Bellemin AL, Munnich A, and Bonaventure J (1997). Mutations of the TWIST gene in the Saethre-Chotzen syndrome. *Nat Genet* **15**, 42–46.

[14] Bourgeois P, Bolcato-Bellemin AL, Danse JM, Bloch-Zupan A, Yoshiba K, Stoetzel C, and Perrin-Schmitt F (1998). The variable expressivity and incomplete penetrance of the twist-null heterozygous mouse phenotype resemble those of human Saethre-Chotzen syndrome. *Hum Mol Genet* **7**, 945–957.

[15] Carver EA, Oram KF, and Gridley T (2002). Craniosynostosis in Twist heterozygous mice: a model for Saethre-Chotzen syndrome. *Anat Rec* **268**, 90–92.

[16] Maestro R, Dei Tos AP, Hamamori Y, Krasnokutsky S, Sartorelli V, Kedes L, Doglioni C, Beach DH, and Hannon GJ (1997). *Twist* is a potential oncogene that inhibits apoptosis. *Genes Dev* **13**, 2207–2217.

[17] Rosivatz E, Becker I, Specht K, Fricke E, Luber B, Busch R, Höfler H, and Becker KF (2002). Differential expression of the epithelial-mesenchymal transition regulators snail, SIP1, and twist in gastric cancer. *Am J Pathol* **161**, 1881–1891.

[18] Fackler MJ, McVeigh M, Evron E, Garrett E, Mehrotra J, Polyak K, Sukumar S, and Argani P (2003). DNA methylation of RASSF1A, HIN-1, RAR-β, cyclin D2 and Twist in *in situ* and invasive lobular breast carcinoma. *Int J Cancer* **107**, 970–975.

[19] Valsesia-Wittmann S, Magdeleine M, Dupasquier S, Garin E, Jallas AC, Combaret V, Krause A, Leissner P, and Puisieux A (2004). Oncogenic cooperation between H-Twist and N-Myc overrides failsafe programs in cancer cells. *Cancer Cell* **6**, 625–630.

[20] Yang MH and Wu KJ (2008). TWIST activation by hypoxia inducible factor-1 (HIF-1): implications in metastasis and development. *Cell Cycle* **7**, 2090–2096.

[21] Le Deley MC, Guinebretière J, Gentet JC, Pacquement H, Pichon F, Marec-Bérard P, Entz-Werlé N, Schmitt C, Brugières L, Vanel D, et al. (2007). SFOP OS94: a randomised trial comparing preoperative high-dose methotrexate plus doxorubicin to high-dose methotrexate plus etoposide and ifosfamide in osteosarcoma patients. *Eur J Cancer* **43**, 752–761.

[22] Polakis P (1997). The adenomatous polyposis coli (APC) tumour suppressor. *Biochem Biophys Acta* **1332**, 127–147.

[23] Cadigan KM and Liu YI (2006). Wnt signalling: complexity at the surface. *J Cell Sci* **119**, 395–402.

[24] Porfiri E, Rubinfeld B, Albert I, Hovanes K, Waterman M, and Polakis P (1997). Induction of a β-catenin–LEF-1 complex by wnt-1 and transforming mutants of β-catenin. *Oncogene* **15**, 2833–2839.

[25] De Lau W, Barker N, and Clevers H (2007). WNT signalling in the normal intestine and colorectal cancer. *Front Biosci* **12**, 471–491.

[26] Stein GS, Lian JB, Van Wijnen AJ, Stein JL, Montecino M, Javed A, Zaidi SK, Young DW, Choi JY, and Pockwinse SM (2004). Runx2 control of organization, assembly and activity of the regulatory machinery for skeletal gene expression. *Oncogene* **23**, 4315–4329.

[27] Kahler RA and Westendorf JJ (2003). Lymphoid enhancer factor-1 and β-catenin inhibit Runx2-dependent transcriptional activation of the osteocalcin promoter. *J Biol Chem* **278**, 11937–11944.

[28] Yousfi M, Lasmoles F, and Marie PJ (2002). TWIST inactivation reduces CBFA1/RUNX2 expression and DNA binding to the osteocalcin promoter in osteoblasts. *Biochem Biophys Res Commun* **297**, 641–644.

[29] Smits R, Van der Houven Van Oordt W, Luz A, Zurcher C, Jagmohan-Changur S, Breukel C, Khan PM, and Fodde R (1998). *Apc*1638N: a mouse model for familial adenomatous polyposis–associated desmoid tumors and cutaneous cysts. *Gastroenterology* **114**, 275–283.

[30] Fodde R, Edelmann W, Yang K, van Leeuwen C, Carlson C, Renault B, Breukel C, Alt E, Lipkin M, Khan PM, et al. (1994). A targeted chain-termination mutation in the mouse Apc gene results in multiple intestinal tumors. *Proc Natl Acad Sci USA* **91**, 8969–8973.

[31] Fodde R, Smits R, Hofland N, Kielman M, and Meera Khan P (1999). Mechanisms of APC-driven tumorigenesis: lessons from mouse models. *Cytogenet Cell Genet* **86**, 105–111.

[32] Kuraguchi M, Edelmann W, Yang K, Lipkin M, Kucherlapati R, and Brown AM (2000). Tumour-associated *Apc* mutations in *Mlh1*–/– *Apc*1638N mice reveal a mutational signature of Mlh1 deficiency. *Oncogene* **19**, 5755–5763.

[33] Dass CR, Ek ET, Contreras KG, and Choong PF (2006). A novel orthotopic murine model provides insights into cellular and molecular characteristics contributing to human osteosarcoma. *Clin Exp Metastatsis* **23**, 367–380.

[34] Thomas DM, Johnson SA, Sims NA, Trivett MK, Slavin JL, Rubin BP, Waring P, McArthur GA, Walkley CR, Holloway AJ, et al. (2004). Terminal osteoblast differentiation, mediated by runx2 and $p27^{KIP1}$, is disrupted in osteosarcoma. *J Cell Biol* **167**, 925–934.

[35] Yoshida T, Phylactou LA, Uney JB, Ishikawa I, Eto K, and Iseki S (2005). Twist is required for establishment of the mouse coronal suture. *J Anat* **206**, 437–444.

[36] Luz A, Müller WA, Linzner U, Strauss PG, Schmidt J, Müller K, Atkinson MJ, Murray AB, Gössner W, Erfle V, et al. (1991). Bone tumour induction after incorporation of short-lived radionuclides. *Radiat Environ Biophys* **30**, 225–227.

[37] Albassam MA, Wojcinski ZW, Barsoum NJ, and Smith GS (2001). Spontaneous fibro-osseous proliferative lesions in the sternums and femurs of B6C3F1 mice. *Vet Pathol* **28**, 381–388.

[38] Mialou V, Philip T, Kalifa C, Perol D, Gentet JC, Marec-Berard P, Pacquement H, Chastagner P, Defaschelles AS, and Hartmann O (2005). Metastatic osteosarcoma at diagnosis: prognostic factors and long-term outcome, the French pediatric experience. *Cancer* **104**, 1100–1109.

[39] Chano T, Matsumoto K, Ishizawa M, Morimoto S, Hukuda S, Okabe H, Kato H, and Fujino S (1996). Analysis of the presence of osteocalcin, S-100 protein, and proliferating cell nuclear antigen in cells of various types of osteosarcomas. *Eur J Histochem* **40**, 189–198.

[40] Fanburg JC, Rosenberg AE, Weaver DL, Lesli KO, Mann KG, Taatjes DJ, and Tracy RP (1997). Osteocalcin and osteonectin immunoreactivity in the diagnosis of osteosarcoma. *Am J Clin Pathol* **108**, 464–473.

[41] Gadwal SR, Gannon FH, Fanburg-Smith JC, Becoskie EM, and Thompson LD (2001). Primary osteosarcoma of the head and neck in pediatric patients: a clinicopathologic study of 22 cases with a review of the literature. *Cancer* **91**, 598–605.

[42] Saldanha G, Ghura V, Potter L, and Fletcher A (2004). Nuclear β-catenin in basal cell carcinoma correlates with increased proliferation. *Br J Dermatol* **151**, 157–164.

[43] Monaghan H, Bubb VJ, Sirimujalin R, Millward-Sadler SJ, and Salter DM (2001). Adenomatous polyposis coli (APC), β-catenin, and cadherin are expressed in human bone and cartilage. *Histopathology* **39**, 611–619.

[44] Won KY, Park HR, and Park YK (2009). Prognostic implication of immunohistochemical Runx2 expression in osteosarcoma. *Tumori* **95**, 311–316.

[45] Lee YY, Van Tassel P, Nauert C, Raymond AK, and Edelken J (1988). Craniofacial osteosarcomas: plain film, CT, and MR findings in 46 cases. *AJR Am J Roentgenol* **150**, 1397–1402.

[46] Laskar S, Basu A, Muckaden MA, D'Cruz A, Pai S, Jambhekar N, Tike P, and Shrivastava SK (2008). Osteosarcoma of the head and neck region: lessons learned from a single-institution experience of 50 patients. *Head Neck* **30**, 1020–1026.

[47] Kim MS, Lee SY, Cho WH, Song WS, Koh JS, Lee JA, Yoo JY, Jung ST, and Jeon DG (2008). Relationships between plain-film radiographic patterns and clinicopathologic variables in AJCC stage II osteosarcoma. *Skeletal Radiol* **37**, 911–1001.